Investigation of the thermal adaptability for a mobile cold atom gravimeter*

Qi-Yu Wang(王启宇)[1], Zhao-Ying Wang(王兆英)[1,†], Zhi-Jie Fu(付志杰)[1], and Qiang Lin(林强)[1,2,‡]

[1] *Institute of Optics, Department of Physics, Zhejiang University, Hangzhou* 310027, *China*

[2] *Center for Optics and Optoelectronics Research, College of Science, Zhejiang University of Technology, Hangzhou* 310023, *China*

(Received 2 June 2016; revised manuscript received 18 August 2016; published online 25 October 2016)

The cold atom gravimeter offers the prospect of a new generation of inertial sensors for field applications. We accomplish a mobile atom gravimeter. With the compact and stable system, a sensitivity of 1.4×10^{-7} g·Hz$^{-1/2}$ is achieved. Moreover, a continuous gravity monitoring of 80 h is carried out. However, the harsh outdoor environment is a big challenge for the atom gravimeter when it is for field applications. In this paper, we present the preliminary investigation of the thermal adaptability for our mobile cold atom gravimeter. Here, we focus on the influence of the air temperature on the performance of the atom gravimeter. The responses to different factors (such as laser power, fiber coupling efficiency, etc.) are evaluated when there is a great temperature shift of 10 °C. The result is that the performances of all the factors deteriorate to different extent, nevertheless, they can easily recover as the temperature comes back. Finally, we conclude that the variation of air temperature induces the increase of noise and the system error of the atom gravimeter as well, while the process is reversible with the recovery of the temperature.

Keywords: atom gravimeter, the environmental adaptability, atom interferometer

PACS: 37.25.+k, 42.60.Lh **DOI:** 10.1088/1674-1056/25/12/123701

1. Introduction

Since the cold-atom-based interferometer was demonstrated first by Chu *et al.*,[1] the field of atom interferometry has developed rapidly. Nowadays, atom interferometry has become one of the most promising tools for ultra-precise measurements of inertial forces,[2–4] physics constants,[5–7] and fundamental physics.[8–10] The instruments relying on the atom interferometer have performed an excellent accuracy and sensitivity for laboratory-based measurements.[11] In recent years, atom interferometry has also displayed prospects for future space-based applications,[12–15] where a micro-gravity environment will allow a long interrogation time, thus increasing the sensitivity by orders of magnitude compared with ground-based devices. For instance, dual-species atom interferometry utilized in the STE-QUEST space mission[16] aims to realize a verification of the equivalence principle at a level of 10^{-15}. Besides, a mobile atom interferometry offers the prospect of a new generation of inertial sensors such as gravimeter and gradiometer, which are dedicated to field applications.[17–19] Recently, the mobile atom interferometry[19,20] have been used to measure the gravity and the initial performance of the apparatus has been estimated. Another gravity measurement in an elevator[18] has been reported with a sensitivity of 42 μGal/Hz$^{1/2}$ (1 Gal = 1 cm/s^2) close to that of the best gravimeters.

In our experiment, we accomplish a mobile cold atom gravimeter for field applications. The major improvement of the instrument is the utilization of a compact laser system, which has a small size but a high stability in contrast to traditional apparatus in laboratory.[21] For this atomic gravimeter, the short-term sensitivity of 1.4×10^{-7} g·Hz$^{-1/2}$ has been acquired. The long-term stability is also evaluated by the tidal measurement of 80 h. However, the present measurement is carried out in a stabilized laboratory environment and using it outside the laboratory remains a challenge. As is well known, the environment elements such as temperature, vibration and magnetic field have direct influences on the high sensitivity and accuracy of an atom interferometer. Several solutions have been presented for these considerations. For example, a thermal control system has been designed to avoid the influence of thermal expansion on the STE-QUEST space mission.[22,23] As for vibration, the passive[24] and active[25] isolation systems have been developed to reject ground vibrations. It is also a good choice to perform the measurements in a low vibration noise environment such as underground galleries.[19] A fluctuating external magnetic field can cause a systematic error for the atom interferometer. In Ref. [23], a shielding design with four individual layers of μ-metal has been tested for the space applications. In our experiment, we utilize a passive vibration isolation platform, which has a good effect on

*Project supported by the National Natural Science Foundation of China (Grant Nos. 11174249 and 61475139), the National High Technology Research and Development Program of China (Grant No. 2011AA060504), the National Basic Research Program of China (Grant No. 2013CB329501), and the Fundamental Research Funds for the Central Universities, China (Grant No. 2016FZA3004).

†Corresponding author. E-mail: zhaoyingwang@zju.edu.cn

‡Corresponding author. E-mail: qlin@zju.edu.cn

© 2016 Chinese Physical Society and IOP Publishing Ltd

the suppression of high frequency vibration. The detailed content is described in Ref. [26]. On the other hand, two layers of permalloy are equipped for shielding against stray magnetic fields. The above two aspects will not be discussed here. In this article, we focus on the influence of the air temperature on the performance of the atom gravimeter.

In this paper, the stability of the atom gravimeter is studied and evaluated when the air temperature changes. In Section 2, the principle of the atom gravimeter and experimental apparatus are described briefly. In Section 3, the detailed experiment procedure and results of the temperature tests are presented. First, the long-term stability of the atom gravimeter is verified by a continuous tidal measurement. Then the influence of the temperature variation is estimated in detail. The responses of different modules to temperature are evaluated with a big temperature shift of 10 °C. Finally, the conclusion of thermal adaptability is given out. The performance of the gravimeter will deteriorate with the variation of temperature, while the process is reversible as the temperature recovers.

2. Principle of atom gravimeter and experimental apparatus

The principle of our cold atom gravimeter has been well illustrated in Ref. [27]. Here, we just describe the fundamental scheme briefly. The gravity acceleration is measured by a Mach-Zehnder type atom interferometer, which is realized by stimulated two-photon Raman transitions between two ground hyperfine levels of ^{87}Rb ($5^2S_{1/2}, F = 1$ and $5^2S_{1/2}, F = 2$). First, we obtain a cloud of cold atoms by magneto–optical trapping in a vacuum chamber. Then the atoms are released and fall freely in the gravitational field. In this stage, the stimulated Raman transitions are induced by a sequence of $\pi/2 - \pi - \pi/2$ Raman pulses. Here, two counter-propagating Raman lasers are utilized to guarantee a large momentum transfer ($2\hbar k$) to the atom. Suppose that all the atoms are in the initial state $5^2S_{1/2}, F = 1$. The atoms are split into two states of $5^2S_{1/2}, F = 1$ and $5^2S_{1/2}, F = 2$ when they interact with the first $\pi/2$ pulse. The second π pulse acts as a mirror to reverse the atoms from one state to the other state. The last $\pi/2$ pulse recombines the two atomic states of different paths, where the two atomic matter waves interfere with each other. Finally, the interference fringe can be acquired. The proportion of atoms P in the state $F = 2$ versus the acceleration g of the atoms along the Raman laser direction of propagation can be given by the formula,

$$P = (1 \pm \cos(\boldsymbol{k}_{\text{eff}} \cdot \boldsymbol{g} - \alpha)T^2)/2, \tag{1}$$

where $k_{\text{eff}} \simeq 4\pi/\lambda$ is the effective wave vector of Raman transition, α is the chirp rate of the Raman laser frequency, which is used to compensate for the Doppler shift due to the accelerated atom motion in the gravitational field, T is the time interval of Raman pulses.

Our experimental apparatus consists of three parts: laser system, electronic system, and gravimeter sensor. The laser system has been comprehensively described in our paper.[21] The schematic diagram is shown in Fig. 1(a). Two distributed feedback (DFB) laser diodes of 1560 nm are used as the master laser and reference laser respectively. The frequency of the reference laser is locked on a rubidium transition, and the frequency of the master laser is locked on the reference one by the method of beat locking. The power of the master laser is amplified by the erbium-doped fiber amplifier (EDFA), and then frequency is doubled in a periodically poled lithium niobate (PPLN) crystal to obtain 1-W laser output with a wavelength of 780 nm. The repumping and Raman lasers are generated by adding a fiber electro–optic modulator (EOM) in the 1560 nm optical path, which produces two sidebands at 6.58 GHz apart from the original frequency. The DFB lasers and the fiber components are integrated together in a standard 19-inch (1 inch = 2.54 cm) cabinet. The remaining optical parts of free space are concentrated on an optical platform. All the lasers of different functions are coupled into the fiber and transported to the gravimeter sensor.

The gravimeter sensor is composed of a traditional magneto–optical trap (2D and 3D MOT), a magnetic shield, a fluorescence collecting system, and a passive vibration isolation platform. The detection region is located about 20 cm under the center of the 3D-MOT.

The detailed experimental procedures are displayed in Fig. 1(b). First, the atoms are pre-cooled in the 2D-MOT, which are immediately transported to the 3D-MOT by a push beam. Up to 9×10^8 cold atoms are loaded in the 3D-MOT within 300 ms. The atoms are then further cooled down to a temperature of 5 μK by a polarization-gradient cooling (PGC). Then, the MOT is switched off and the atoms fall freely in the gravitational field. In this stage, the atoms are selected in the state of $F = 2$, $m_F = 0$ by using two microwave pulses and a blow pulse. After that a Raman laser π pulse acts on the atoms to obtain a narrow vertical velocity distribution in the state of $F = 1$, $m_F = 0$. In the next stage, a matter wave interferometer is fulfilled by a sequence of three Raman pulses of durations 8 μs, 16 μs, 8 μs respectively. The time interval between two continuous Raman pulses T is 60 ms. Finally, the detection system is used to collect the fluorescence of the atoms in the state of $F = 2$ and $F = 1$, respectively. The interference fringe can be acquired by scanning the chirp rate α. The gravity value can be extracted from the phase of the fringe.

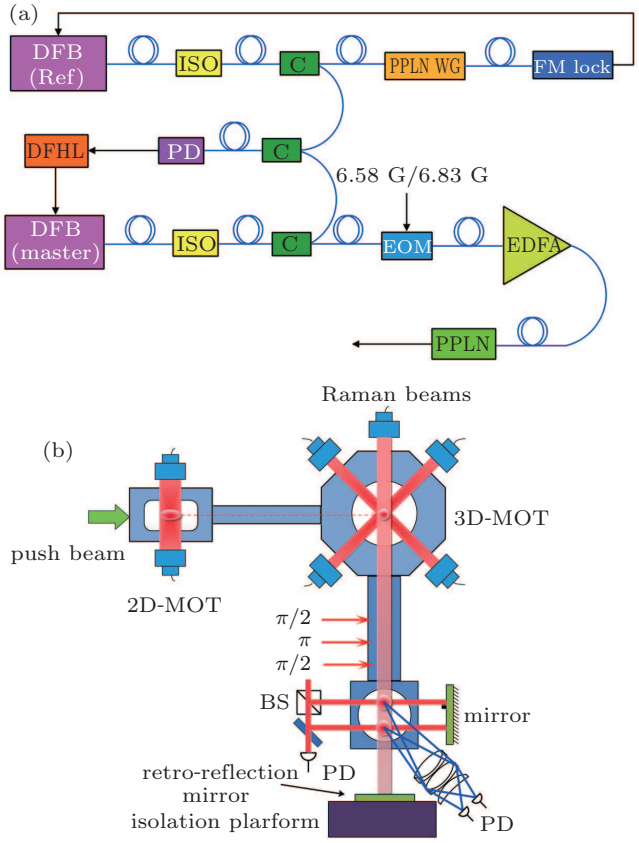


Fig. 1. (color online) The experimental schematic diagram: (a) the laser system;[21] (b) the gravimeter sensor.

3. Experimental procedure and results

In order to estimate the influence of the air temperature and eliminate the disturbances of other factors, we should first give out the long-term stability of our gravimeter at a steady temperature in the laboratory. We acquire the long-term stability of gravity monitoring by the tidal measurement. A continuous measurement of 80 h was operated from 12 December to 15 December 2015. The experimental data are shown in Fig. 2. The time interval between two continuous Raman pulses T is 60 ms. The experimental data coincide well with those of the theoretical tide model of the Earth. The residual can be obtained by subtracting the theoretical model from the experimental data, which is shown in Fig. 2. The uncertainty of the residual mainly comes from the vibration noise. That is because our laboratory is located in the urban area, where there is more human activities. The Allan deviation of the gravity measurement could be derived from the residual as shown in Fig. 3. The short-term sensitivity of 1.4×10^{-7}g·Hz$^{-1/2}$ can be acquired from the red solid line in the figure. After a long integration time of 2000 s, the resolution is better than 6 μGal.

In order to implement the outdoor gravity measurement by using the atom gravimeter in the future, it is necessary to perform the environment tests to verify its compatibility with field applications. Here, we investigate mainly the influence of air temperature on the gravimeter.

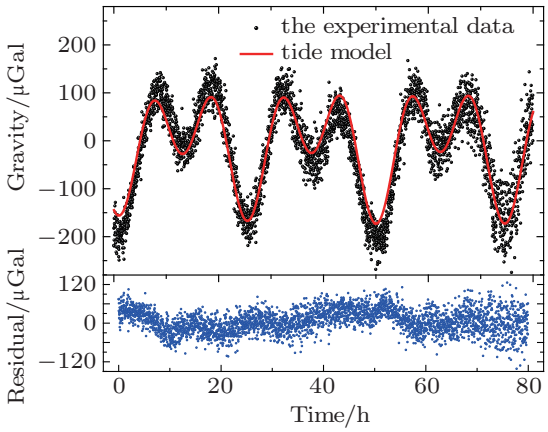


Fig. 2. (color online) Tidal measurement of 80 h from 12 to 15 December 2015. The black dots represent the experimental data, the red line refers to the theoretical tide model of the Earth. The blue dots in the bottom represent the residuals by subtracting the data of the tide model from the experimental data.

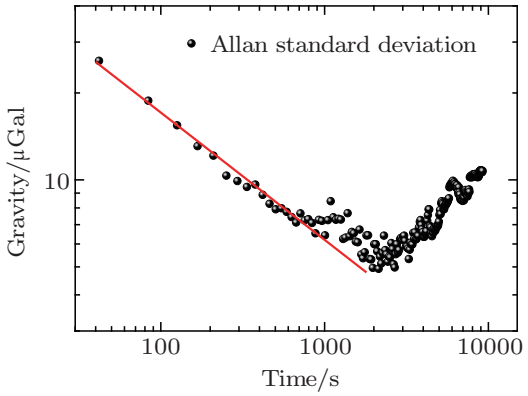


Fig. 3. (color online) Allan deviation of the gravity measurement.

The effect of the air temperature is mainly due to the expansion and contraction of the optical devices, which directly leads to the deviation of the optical path and the variation of physical dimensions, thus changing the efficiency of PPLN frequency doubled and the fiber coupling efficiency. Besides, the characteristics of electric devices and atom gas may also change to different extents. The control of the temperature is fulfilled by the central air-conditioner. The variation is a continuous and slow process in a range of 10 degrees centigrade.

Due to the utilization of the DFB laser diode with a high performance controller, the output power and frequency of the 1560-nm laser is quite stabilized. However, the efficiency of the frequency doubled is very sensitive to temperature, even if an oven is used for controlling the temperature of the PPLN crystal. We design a locking system to guarantee the stability of laser power after frequency has been doubled by controlling the driver power of an acoustic optical modulator (AOM). The details have been described in our previous paper.[21] A laser power instability of 6×10^{-3} is reached after the system has been locked with a measuring time of 9 h under normal temperature. Here, we estimate its performance when there is a great temperature shift of 10 °C. The results are presented in Fig. 4. At the beginning, we adjust the air conditioner and

make the temperature rise rapidly near 10 °C in the first hour. Then we make the temperature return to the original state in a slow process. After that we repeat the modulation process several times. Meanwhile, we record the synchronous temperature variation of the PPLN crystal oven. As seen in Fig. 4, the laser power is out of locking as the air temperature varies significantly. The laser power increases about 4%, where there is a time delay as a result of heat conduction. However, the laser power can return automatically to the initial state as the temperature falls down. From the bottom of the figure, we can see that the temperature variation of the PPLN crystal oven is the main reason for the variation of the laser power.

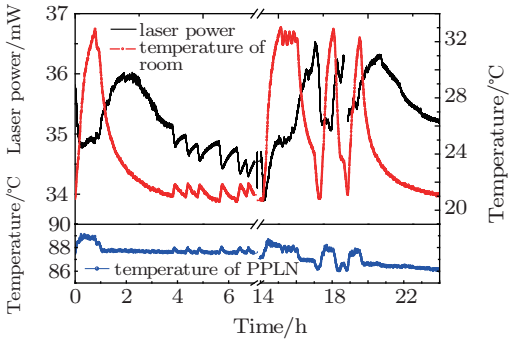


Fig. 4. (color online) The laser output power measured with the variation of temperature. The red curve is the variation of temperature which is recorded by a temperature sensor. The black curve is the variation of the output laser power after power locking. The blue curve in the bottom shows the temperature variation of the PPLN crystal oven.

The second factor we will estimate is the coupling efficiency of the fiber. When the temperature varies, a certain deformation will happen to the fiber coupler as well as the optical and mechanical devices, which affects the fiber output power. Here, we use the ratio η ($\eta = P_{\text{output}}/P_{\text{input}}$) to represent the coupling efficiency, where the P_{input} and P_{output} are the input and output laser power of the fiber, respectively. In this test, the temperature is also controlled by the air conditioner with a range of 10 °C. The input and output laser power are recorded by the optical power meter respectively. The results are given in Fig. 5. Figure 5(a) shows the variations of input and output laser power. It can be seen that both of them tend to decrease due to the drop of the doubled efficiency of the PPLN crystal. Figure 5(b) shows the variation of the ratio η. The value of η declines by 5% with the increase of temperature. Furthermore, the process is irreversible, that is to say, η cannot be back automatically to the original value when the temperature returns. Nevertheless, we can recover it easily by turning the screws on the reflector mount or fiber coupler.

Besides, we also investigate the polarization characteristics of the output beam from fiber at different temperatures. The fiber used is polarization-maintaining single mode patch cable. The cables and fiber couplers are all purchased from OZ Optics. A polarization analyzer is employed in this test. A polarization beam splitter is placed in front of the fiber coupler to exclude the influence of other factors, which acts as a polarization filter. We estimate the polarization performances at 22 °C and 30 °C respectively, and the result is that the polarization property of the output beam from fiber is not sensitive to temperature.

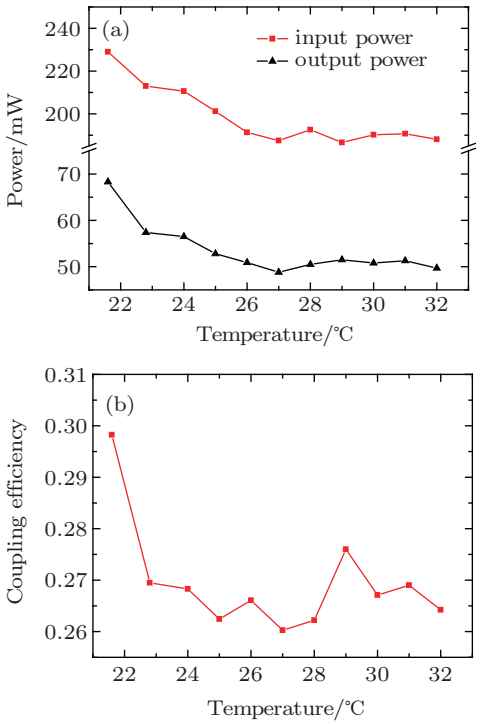


Fig. 5. (color online) Variations of (a) input and output power and (b) the coupling efficiency of optical fiber with temperature.

Then we will discuss the influence of the air temperature on atom number in the state preparation process. The atom number of the $F = 2$ state and the normalized value in the 3D-MOT are recorded separately. The temperature-dependent curves are both shown in Fig. 6. As seen from Fig. 6, there is a direct correlation between the atom number and the temperature, but there is a time delay between them. When there is a great temperature shift of 10 °C, the variation of the atom number of the $F = 2$ state is more than 50%, while the variation range of the normalized value is less than 10%. The reason for the results mainly comes from two aspects. One is that when the temperature rises, the saturated vapor pressure of rubidium in the vacuum chamber also changes, which makes an increase of atom density, thus increasing the trapped atom numbers of both state $F = 2$ and $F = 1$ in the MOT; the other is that the coupling efficiency of the fiber declines as the elevation of the temperature, which causes atom number to decrease.

Finally, we investigate the influence of the air temperature on the interference fringes of atomic population. The fringe contrast is an important parameter which affects the sensitivity of the gravity measurement, so we study the fringe contrast curve as the temperature changes in Fig. 7(a). The fringe contrast decreases when the temperature rises, but it returns to the original value with the recovery of air temperature. The main

reason for the variation is that the power of the Raman beam decreases when the temperature rises, thus leading to the alteration of the Raman π pulse length. By the cosine fitting of the fringes, we can also obtain the synchronous sensitivity variation of the gravity measurement, which is shown in Fig. 7(b). As seen from the figure, the sensitivity also turns worse when the temperature rises, which is not regular in the whole process. Nevertheless, when the air temperature comes back to the original state, the sensitivity of the gravity measurement can be recovered automatically.

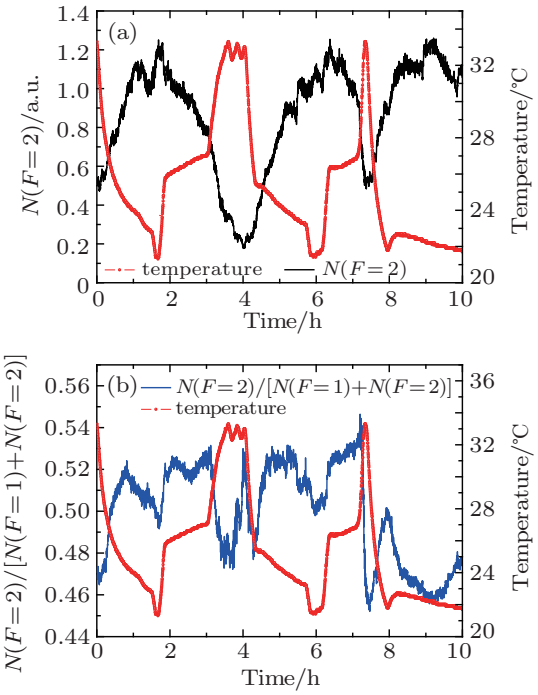


Fig. 6. (color online) Variations of (a) atom numbers of $F=2$ state and (b) the normalized value of atom numbers in $F=2$ state and temperatures with time. Both of the variables are specified as $N(F=2)$ and $N(F=2)/(N(F=1)+N(F=2))$ in the figure.

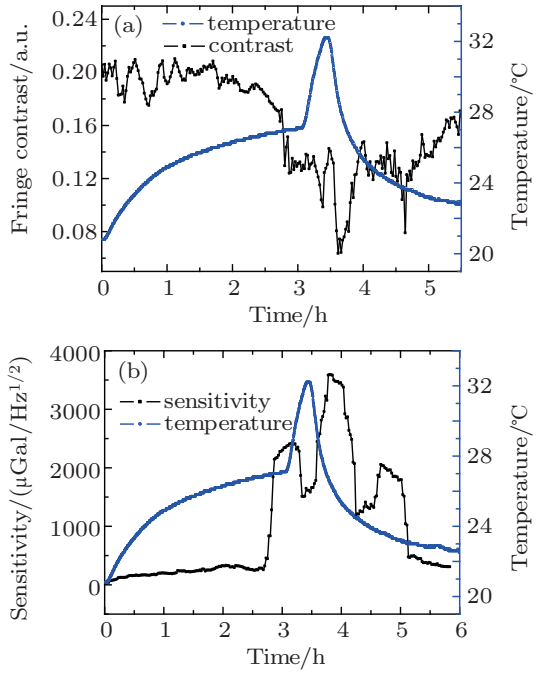


Fig. 7. (color online) (a) Curves of fringe contrast (black) and temperature (blue) with time. (b) Curves of sensitivity (black) and temperature (blue) with time.

For a comprehensive analysis of the fringe variation in the process of temperature modulation, we select several fringes in a temperature range from 22 °C to 32 °C in steps of 2 °C in the above experiment process, which are presented in Fig. 8. The corresponding cosine fitting curves are also shown in the figure. When the temperature rises, the most prominent feature is the reduction of the fringe amplitude, which is consistent with the behaviors of the curves in Fig. 7(a). Moreover, the noise and a phase shift of the fringes increase, which causes the noise and system errors of the gravity measurement to increase, while the process is reversible.

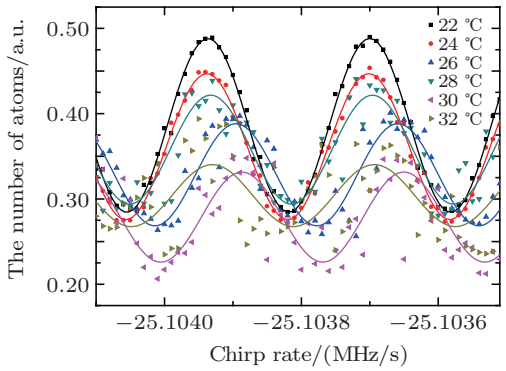


Fig. 8. (color online) Variations of the number of atoms with chirp rate for $T=60$ ms at different environment temperatures.

4. Conclusions

In this work, a sensitivity of 1.4×10^{-7} g·Hz$^{-1/2}$ is achieved with our transportable atom gravimeter. Moreover, the long-term stability is demonstrated by a continuous gravity measurement of 80 h. We present the preliminary investigation on the thermal adaptability for our gravimeter. In particular, the influence of the temperature variation is estimated in detail. The responses of different modules to the temperature are evaluated with a big temperature shift of 10 °C. As a result, the performances of all the modules deteriorate to different extents, nevertheless, they can easily recover as the temperature comes back. The variation of air temperature induces the increase of noise and system errors of the atom gravimeter, while the process is reversible with the recovery of the temperature. The work provides the basis for using our atom gravimeter outside of the laboratory. Meanwhile, it means one step closer to field applications in the future.

References

[1] Kasevich M and Chu S 1991 *Phys. Rev. Lett.* **67** 181
[2] Gustavson T L, Bouyer P and Kasevich M A 1997 *Phys. Rev. Lett.* **78** 2046
[3] Kasevich M and Chu S 1992 *Appl. Phys. B* **54** 321
[4] Zhou L, Xiong Z Y, Yang W, Tang B, Peng W C, Wang Y B, Xu P, Wang J and Zhan M S 2011 *Chin. Phys. Lett.* **28** 013701
[5] Fixler J B, Foster G T, McGuirk J M and Kasevich M A 2007 *Science* **315** 74

[6] Wicht A, Hensley J M, Sarajlic E and Chu S 2002 *Phys. Scr.* **2002** 82
[7] Holmgren W F, Revelle M C, Lonij V P and Cronin A D 2010 *Phys. Rev. A* **81** 053607
[8] Müller H, Peters A and Chu S 2010 *Nature* **463** 926
[9] Hohensee M, Lan S Y, Houtz R, Chan C, Estey B, Kim G, Kuan P C and Müller H 2011 *Gen. Relativ. Grav.* **43** 1905
[10] Herrmann S, Dittus H and Lämmerzahl C 2012 *Class. Quantum Grav.* **29** 184003
[11] Hu Z K, Sun B L, Duan X C, Zhou M K, Chen L L, Zhan S, Zhang Q Z and Luo J 2013 *Phys. Rev. A* **88** 043610
[12] Yu N, Kohel J M, Kellogg J R and Maleki L 2006 *Appl. Phys. B* **84** 647
[13] Hogan J M, Johnson D M, Dickerson S, Kovachy T, Sugarbaker A, Chiow S W, Graham P W, Kasevich M A, Saif B and Rajendran S 2011 *Gen. Relativ. Grav.* **43** 1953
[14] Tino G M, Sorrentino F, Aguilera D, Battelier B, Bertoldi A, Bodart Q, Bongs K, Bouyer P, Braxmaier C and Cacciapuoti L 2013 *Nucl. Phys. B (Proc. Suppl.)* **243** 203
[15] Geiger R, Méoret V, Stern G, Zahzam N, Cheinet P, Battelier B, Villing A, Moron F, Lours M and Bidel Y 2011 *Nat. Commun.* **2** 474
[16] Aguilera D, Ahlers H, Battelier B, Bawamia A, Bertoldi A, Bondarescu R, Bongs K, Bouyer P, Braxmaier C and Cacciapuoti L 2014 *Class. Quantum Grav.* **31** 115010
[17] Schmidt M, Senger A, Hauth M, Freier C, Schkolnik V and Peters A 2011 *Gyroscopy Navig.* **2** 170
[18] Bidel Y, Carraz O, Charri'ere R, Cadoret M, Zahzam N and Bresson A 2013 *Appl. Phys. Lett.* **102** 144107
[19] Farah T, Guerlin C, Landragin A, Bouyer P, Gaffet S, Dos Santos F P and Merlet S 2014 *Gyroscopy Navig.* **5** 266
[20] Hauth M, Freier C, Schkolnik V, Senger A, Schmidt M and Peters A 2013 *Appl. Phys. B* **113** 49
[21] Wang Q Y, Wang Z Z, Fu Z J, Liu W Y and Lin Q 2016 *Opt. Commun.* **358** 82
[22] Schuldt T, Schubert C, Krutzik M, Bote L G, Gaaloul N, Hartwig J, Ahlers H, Herr W, Posso-Trujillo K and Rudolph J 2015 *Exp. Astron.* **39** 167
[23] Milke A, Kubelka-Lange A, Guerlebeck N, Rievers B, Herrmann S, Schuldt T and Braxmaier C 2014 *Rev. Sci. Instrum.* **85** 083105
[24] Le Gouët J, Mehlstäubler T E, Kim J, Merlet S, Clairon A, Landragin A and Dos Santos F P 2008 *Appl. Phys. B* **92** 133
[25] Zhou M K, Duan X C, Chen L L, Luo Q, Xu Y Y and Hu Z K 2015 *Chin. Phys. B* **24** 050401
[26] Wu B, Wang Z Y, Cheng B, Wang Q Y, Xu A P and Lin Q 2014 *Metrologia* **51** 452
[27] Peters A, Chung K Y and Chu S 2001 *Metrologia* **38** 25